Constant Current Charging and Transfer Efficiency Improvements for a Dynamic Wireless Charging System

Nguyen Thi Diep
Faculty of Control and Automation, Electric Power University, Vietnam
diepnt@epu.edu.vn

Tran Duc Hiep
School of Electrical and Electronic Engineering, Hanoi University of Science and Technology, Vietnam | Faculty of Electrical Engineering, Hanoi University of Industry, Vietnam
tranduchiep@haui.edu.vn

Nguyen Kien Trung
School of Electrical and Electronic Engineering, Hanoi University of Science and Technology Vietnam
trung.nguyenkien1@hust.edu.vn (corresponding author)

Received: 23 August 2023 | Revised: 16 October 2023 | Accepted: 29 October 2023

 DOI: https://doi.org/10.48084/etasr.6315

ABSTRACT

Dynamic Wireless Charging (DWC) systems for electric vehicles (EVs) are being studied and developed for wide applications. To ensure a long life for lithium-ion batteries, Constant Current (CC) charging is required. However, the equivalent load of the battery changes during CC charging, which reduces the system's efficiency. To solve that problem, this paper proposes a new control method that combines CC charging and improves transfer efficiency using only an active rectifier on the secondary side of the DWC system. Moreover, this study also proposes a method to estimate the coupling coefficient through the parameters measured on the secondary side without the need for wireless communication between the two sides. A model of a 1.5 kW DWC system with a transfer distance of 150 mm was built in a laboratory to verify the accuracy of the proposed method. The results showed that the charging current reached the required value, and the maximum system efficiency was 85%.

Keywords-constant current charge; improved efficiency; dynamic wireless charging system; electric vehicle

I. INTRODUCTION

Electric Vehicles (EVs) are environmentally friendly means of transport. To make the use of EVs more convenient and safer, many problems related to EVs are currently being studied and developed [1-3]. Wireless charging technology for EVs is attractive because it simplifies the power supply process and eliminates some of the dangers of electrical leakage for users. Research is directed toward applying wireless charging technology to charge EVs while they are in motion because it can reduce battery weight and increase travel distance [4-6]. Today, EVs mainly use lithium-ion batteries due to their large energy density, long life, and safety [7]. To prolong the battery life, the CC charging mode is required. However, during CC charging, the equivalent load impedance of the battery varies, which reduces the system's efficiency [8]. A challenge is how to achieve CC charging mode and ensure high system efficiency.

Due to the complexity of wireless charging systems, it is difficult to achieve both the above criteria. Several studies attempted to achieve either of these two criteria. Some studies focused on improving the efficiency system. Commonly used methods are impedance matching circuit design [9-10], DC/DC converter control to convert load impedance [11-13], and minimum input current/power point detection to maximize transfer efficiency [14-15]. However, these studies have not addressed the charge control problem. Some studies focused on the control of the CC/CV charging process. In [16], an LCCC/S compensation circuit structure and parameter adjustment method were proposed to achieve CC and CV at two ZPA frequencies. This method is unsuitable for dynamic charging systems where various types of electric vehicles operate. In a Static Wireless Charging (SWC) system, CC and CV charging modes are achieved at two different frequencies by designing the coil and compensating circuit [17]. This design method is complicated, and the system requires wireless communication between the two sides to control the charging process. In the

WPT system, CC and CV charging modes are achieved by phase shift modulation of the primary side inverter [18]. However, on the secondary side, the compensation circuit must be switched from series to parallel when switching the charging mode from CC to CV. This method is only suitable for applications with compact and lightweight receivers.

Some studies have proposed combining CC charge control with improved transfer efficiency in SWC systems. In [19-20], the secondary active rectifier phase shift modulation method was used to realize the CC charging mode. Maximum transfer efficiency tracking is based on finding the minimum DC input current point through the perturbation and observation algorithm. The disadvantage of this system is that the semi-active rectifier and the inverter can operate stably. Furthermore, this method is unsuitable for DWC systems because the working point detection time is high. In [21], a dual-phase shift modulation method was used to keep output voltage and current constant while improving the efficiency of WPT systems. However, as this system requires wireless communication between the two sides, it is not suitable for DWC systems.

To solve the above problems, this paper proposes a control method that combines CC charging and improves efficiency using only an active rectifier on the secondary side. CC is required from the Battery Management System (BMS). The efficiency optimization algorithm was implemented based on the equivalent load impedance control method that follows the optimal load impedance value and limits the required charging current. Then, the closed-loop controller was designed to CC charging. Moreover, a method for estimating the coupling coefficient in the DWC system is also presented. Therefore, the system does not need to use wireless communication between the two sides.

II. STRUCTURE AND CHARACTERISTICS OF THE PROPOSED DWC SYSTEM

A. System Structure

Figure 1 shows the structure of the proposed DWC system. Three transmitting coils are placed side by side to create the charging lane on the primary side. An 85 kHz inverter consisting of four MOSFETs from S1 to S4 powers the transmitting coils through the compensation circuit. On the secondary side, the receiving coil is mounted under the EV to receive power from the wireless charging lane. The receiving coil induces an alternating voltage through the compensating circuit feeds to the active rectifier. The active rectifier consists of 4 MOSFETs, Q1 to Q4, which provide charging power for the battery. The LCC compensation circuit is designed for both the primary and secondary sides.

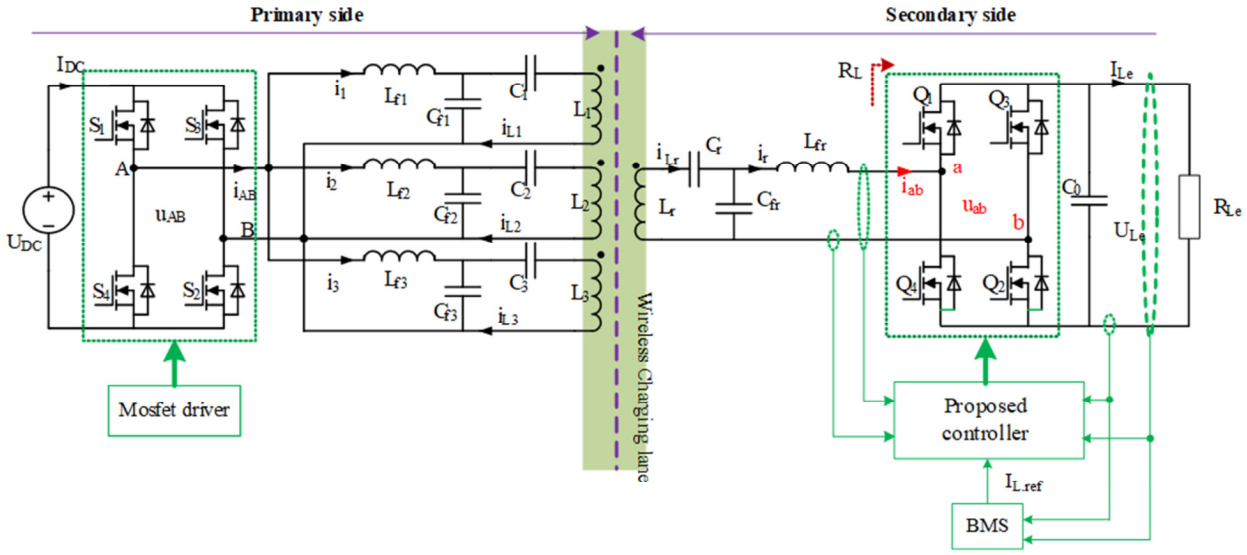

Fig. 1. The proposed dynamic wireless charging system.

B. Characteristics of the Coupling Coefficient in the Proposed DWC System

This study used finite element analysis simulation to design the transmitting and receiving coils to reduce power pulsation [22]. Each coil consists of three layers: the Litz wire layer, the ferrite layer, and the aluminum shield layer. The primary side consists of three transmitting coils (T1, T2, and T3) placed side by side under the wireless charging lane. The receiving coil is mounted under the EV. The transfer distance is equal to 150 mm. Figure 2 shows the structure of the coils in the DWC system.

The receiver position in the x direction is denoted by p_x, and in the y direction is denoted by p_y. The receiving coil is centered on the first transmitting coil (T1), (p_x, p_y) = (0, 0). Figure 3 shows the EFA simulation results of the coupling coefficient when the receiver moves along the wireless charging lane in three cases. In case 1, when the receiver moves along the charging lane (d_x is from 0 to 800 mm) and d_y is 0 mm (no lateral misalignment), the average coefficient coupling (k_r) is equal to 0.14. In case 2, when d_x is from 0 to 800 mm and d_y is 40 mm (lateral misalignment 40 mm), k_r is equal to 0.111. In case 3, when d_x is from 0 to 800 mm and d_y is

60 mm (lateral misalignment 60 mm), k_r is equal to 0.078. Thus, it can be concluded that the coupling coefficient depends on the position of the receiving coil. When the receiver moves, the total coupling coefficient changes. When the lateral misalignment increases, the total coupling coefficient decreases.

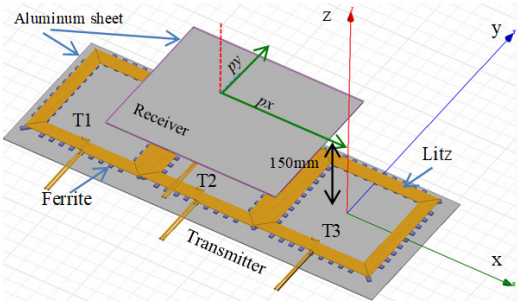

Fig. 2. Structure of the coils in the DWC system.

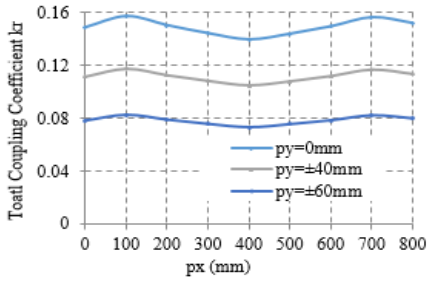

Fig. 3. The total coupling coefficient.

C. Transfer Efficiency Characteristics Analysis

The dual-side LCC compensation circuit was designed for this system [22]. Figure 4 shows the equivalent circuit diagram from the inverter output on the primary side to the battery on the secondary side. The equivalent load impedance seen from the active rectifier side to the battery is called R_L.

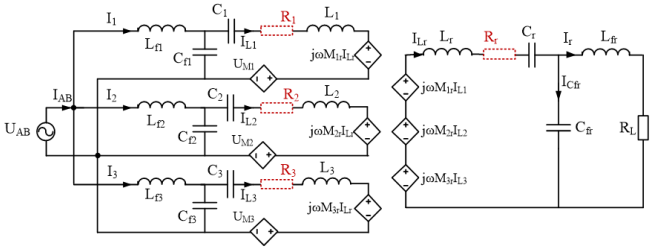

Fig. 4. Equivalent circuit diagram.

Transfer efficiency is calculated as follows [22]:

$$\eta = \frac{R_L I_r^2}{R_L I_r^2 + R_r I_{Lr}^2 + R_1 I_{L1}^2 + R_2 I_{L2}^2 + R_3 I_{L3}^2} = \frac{R_L}{R_L^2 \frac{R_r}{\omega^2 L_{fr}^2} \frac{3+k_r^2 Q_i Q_r}{k_r^2 Q_i Q_r} + R_L \left(1 + \frac{6}{k_r^2 Q_i Q_r}\right) + \frac{3\omega^2 L_{fr}^2}{R_r} \frac{1}{k_r^2 Q_i Q_r}} \quad (1)$$

where $Q_i = \omega L_i / R_i$ and $Q_r = \omega L_r / R_r$ is the coil quality factor. R_1, R_2, R_3, and R_r are the resistances of the transmitting and receiving coils, respectively. Equation (1) shows that the transfer efficiency depends on the changing parameters during dynamic charging, which are k_r and R_L. While k_r depends on the position of the EV, R_L depends on the state of charge of the battery. Assuming that the value of k_r is known, the transfer efficiency depends only on R_L. To find the maximum transfer efficiency, the following system of equations must be solved:

$$\begin{cases} \frac{\partial \eta}{\partial R_L} = 0 \\ \frac{\partial \eta^2}{\partial R_L^2} < 0 \end{cases} \quad (2)$$

The maximum transfer efficiency is obtained as follows:

$$\eta_{max} = \frac{k_r^2 Q_i Q_r}{\left(\sqrt{3} + \sqrt{3 + k_r^2 Q_i Q_r}\right)^2} \quad (3)$$

The value of the equivalent load impedance is equal to:

$$R_L = R_{L.opt} = \frac{\omega^2 L_{fr}^2}{R_r} \sqrt{\frac{3}{3 + k_r^2 Q_i Q_r}} \quad (4)$$

where $R_{L.opt}$ is called optimal impedance, and $R_{L.opt}$ depends on the total coupling coefficient k_r. Equations (3) and (4) show that when $R_L = R_{L.opt}$, transfer efficiency is maximum.

Moreover, as seen above, k_r changes when the receiver moves, and in combination with (4) it is found that the value of $R_{L.opt}$ changes and depends on the receiver's position. Therefore, for maximum transfer efficiency, it is necessary to control R_L according to the $R_{L.opt}$ value. The coupling coefficient value needs to be estimated when the EVs move.

D. Estimation of the Coupling Coefficient by the Parameters Measured on the Secondary Side

The currents across the transmitting coils [22] are:

$$I_{L1} = I_{L2} = I_{L3} = I_{Li} = -\frac{U_{AB}}{1/(j\omega C_{fi})} = -j\omega C_{fi} U_{AB} \quad (5)$$

On the secondary side, the relationship among the parameters is:

$$\begin{cases} \left(j\omega L_r + R_r + \frac{1}{j\omega C_r}\right) I_{Lr} + \frac{1}{j\omega C_{fr}} I_{Cfr} = j\omega M_r I_{Li} \\ \left(j\omega L_{fr} + R_L\right) I_r = \frac{1}{j\omega C_{fr}} I_{Cfr} \\ I_{Cfr} = I_{Lr} - I_r \end{cases} \quad (6)$$

From (5) and (6), the calculation expression k_r is drawn:

$$k_r = \frac{L_{fr}}{U_{AB}\sqrt{L_i L_r}} \left[\frac{R_r}{\omega L_{fr}} U_{ab} + \omega L_{fr} I_{ab}\right] \quad (7)$$

where U_{AB} is the RMS of the output voltage of the primary side inverter, and U_{ab} and I_{ab} are the RMS of the input voltage and current of the active rectifier on the secondary side. Thus, if U_{AB} is not adjusted or is constant, k_r can be estimated by measuring the value of U_{ab} and I_{ab}. This means that k_r can be estimated using only the parameters measured on the secondary side.

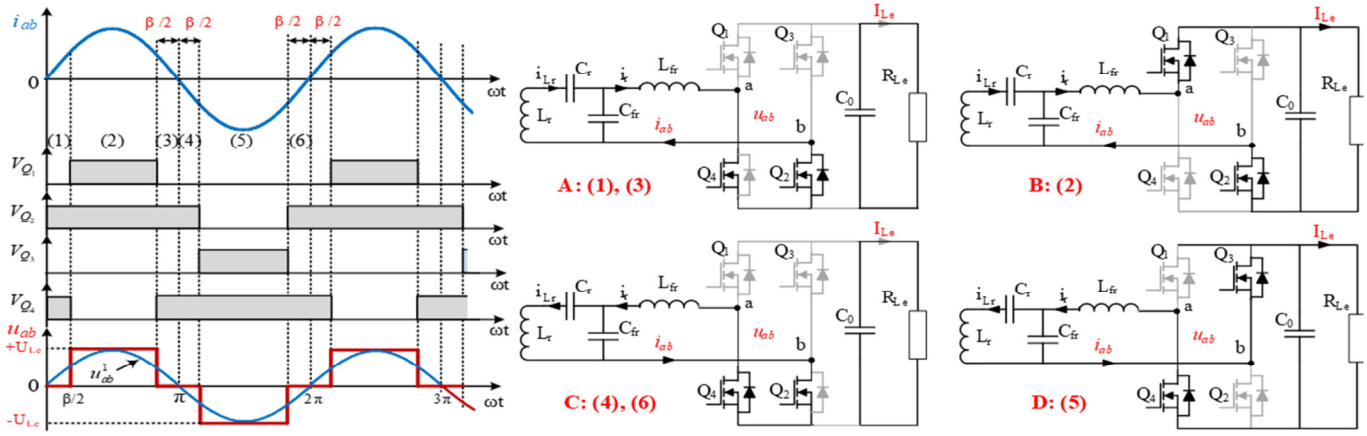

(a) (b)

Fig. 5. (a) Mosfet control signal, (b) MOSFET on/off state.

III. CC CHARGING AND IMPROVED EFFICIENCY WITH SECONDARY ACTIVE RECTIFIER PHASE SHIFT CONTROL

A. The Working Principle of the Proposed Active Rectifier

Active rectifier phase shift modulation was used to achieve both CC charging and efficiency improvement goals. The secondary active rectifier is controlled by methods of symmetric phase shift combined with phase synchronization. For the equivalent load impedance to be purely resistive, the input voltage and current of the active rectifier must be in phase. Then, phase shift modulation is performed to control the CC charging combined with impedance matching to improve the system's efficiency.

Figure 5 shows the waveforms and switching states of the active rectifier. u^1_{ab} and i^1_{ab} are the fundamental wave components of the input voltage and current of the active rectifier. $V_{Q1} \div V_{Q4}$ is the open signal of MOSFETs from Q_1 *to* Q_4. The MOSFETs on the signal are synchronized with the zero moments of i^1_{ab}. MOSFETs from Q_1 to Q_4 operate at the resonant frequency. During one cycle, the current i_{ab} has negative and positive directions. At each cycle, there are four switching states of the IGBTs corresponding to six different stages, as shown in Figure 5(b).

State A, corresponds to phases (1) and (3), where Q_2 and Q_4 are on. Current i_{ab} flows through Q_2 and Q_4, and no energy is transferred to the load. Therefore, u_{ab} and I_{Le} are zero. Energy has been accumulated in the capacitor C_0 fed to the load. State B, corresponds to phase (2), where Q_1, Q_2 are on. Current i_{ab} flows to the load through Q_1 and Q_2. u_{ab} is equal to U_{Le}, I_{Le} is equal to i_{ab}, and energy is transferred to the load. In state C, phases (4) and (6), and in state D, phase (5), the analysis is the same as in states A and B. Thus, in one duty cycle, u_{ab} has the following values:

$$u_{ab} = \begin{cases} 0: 0 < \omega t < \beta/2 \\ U_{Le}: \beta/2 < \omega t < \pi - \beta/2 \\ 0: \pi - \beta/2 < \omega t < \pi + \beta/2 \\ -U_{Le}: \pi + \beta/2 < \omega t < 2\pi - \beta/2 \end{cases} \quad (8)$$

where β is the phase shift angle, and U_{Le} is the output voltage of the active rectifier. Based on the fundamental harmonic method, U_{ab} is calculated by:

$$U_{ab} = \frac{2\sqrt{2}}{\pi} U_{Le} cos\frac{\beta}{2} \quad (9)$$

The charging current is calculated as follows:

$$I_{Le} = \frac{2\sqrt{2}}{\pi} I_{ab} cos\frac{\beta}{2} \quad (10)$$

Equation (10) shows that, when adjusting the β angle, the charging current can be controlled by a constant. Assuming that the reference charging current I_{Le} is known and I_{ab} is measured, the phase-shift angle β is determined by:

$$\beta = 2acos\left(\frac{\pi}{2\sqrt{2}}\frac{I_{Le}}{I_{ab}}\right) \quad (11)$$

Based on the power balance condition, R_{Le} is calculated by:

$$R_L = \frac{8}{\pi^2} R_{Le} \left(cos\frac{\beta}{2}\right)^2 \quad (12)$$

Thus, when R_{Le} changes according to the charging state of the battery, changing the phase shift angle β will adjust the value of the equivalent impedance R_L. Therefore, it is possible to control the equivalent load impedance according to the optimal load impedance. An expression can be derived from (12) to calculate the phase shift angle when R_L and R_{Le} are known:

$$\beta = 2acos\left(\sqrt{\frac{R_L}{\frac{8}{\pi^2}R_{Le}}}\right) \quad (13)$$

These equations show that as the phase shift angle changes, the charging current and the load impedance vary accordingly.

B. The Proposed Control Structure

During the charging process, the BMS will calculate and decide the charging current value for the battery. The reference charging current is $I_{L.ref}$, and the tolerable charging fluctuation rate is δ. Thus, the current limit in the CC charging mode is:

$$\begin{cases} I^+_{L.ref} = I_{L.ref}(1+\delta) \\ I^+_{L.ref} = I_{L.ref}(1-\delta) \end{cases} \quad (14)$$

Figure 6 shows the block diagram of the CC charging control combined with optimal impedance tracking to improve efficiency. The referent charging current ($I_{Le.ref}$) is given from the BMS. The RMS of the input voltage/current (U_{ab}/I_{ab}) and the output voltage/current (U_{Le}/I_{Le}) of the active rectifier are measured. k_r is estimated by (7), from which the $R_{L.opt}$ can be calculated according to (4). Substituting $R_{L.opt}$ into (13) will find the optimal phase shift angle (β_{opt}). Substituting the optimal phase shift angle (β_{opt}) into (10) will provide the optimal current charging ($I_{Le.opt}$). On the other hand, the limits of the phase shift angle [β_{min}, β_{max}] can be calculated from (14) and (11). Next, the limit on the equivalent load impedance [$R_{L.min}$, $R_{L.max}$] is calculated according to (12). Finally, the efficiency optimization algorithm is implemented with the inputs $I_{Le.opt}$, $R_{L.opt}$, $R_{L.min}$, $R_{L.max}$, $I^{+}_{Le.ref}$, $I^{-}_{Le.ref}$.

Figure 7 shows the flow chart of the efficiency optimization algorithm. The closed-loop controller is used to control the CC charging mode. The referent charging current is given from the efficiency optimization algorithm. If $R_{L.opt}$ is greater than $R_{L.min}$ and less than $R_{L.max}$, the system performs $I_{Le.opt}$ as the reference current for the current controller. If $R_{L.opt}$ is greater than $R_{L.max}$, the system performs $I^{+}_{Le.ref}$ as the reference current for the current controller. If $R_{L.opt}$ is less than $R_{L.min}$, the system performs $I^{-}_{Le.ref}$ as the reference current for the current controller. Based on the errors, the PI calculates the β for the active rectifier. In addition, the PLL circuit is used to determine when i^{l}_{ab} crosses zero. The synchronization signal is sent to the phase shift modulator to open the IGBT *Q1* to *Q4*. To design the controllers, the transfer function of the system needs to be determined. However, with resonant converters with many capacitors and inductors as in this system, the modeling to find the transfer function is very complicated. Therefore, this study used the model recognition method on the PSIM software to identify the transfer function (15). The PI controller is designed as in (16).

$$G_{\beta I} = \frac{1.05*10^{10}s+6.922*10^{14}}{s^3+6.945*10^5 s^2+1.948*10^{11}s+1.242*10^{16}} \quad (15)$$

$$G_c = -200 - \frac{60118.4115}{s} \quad (16)$$

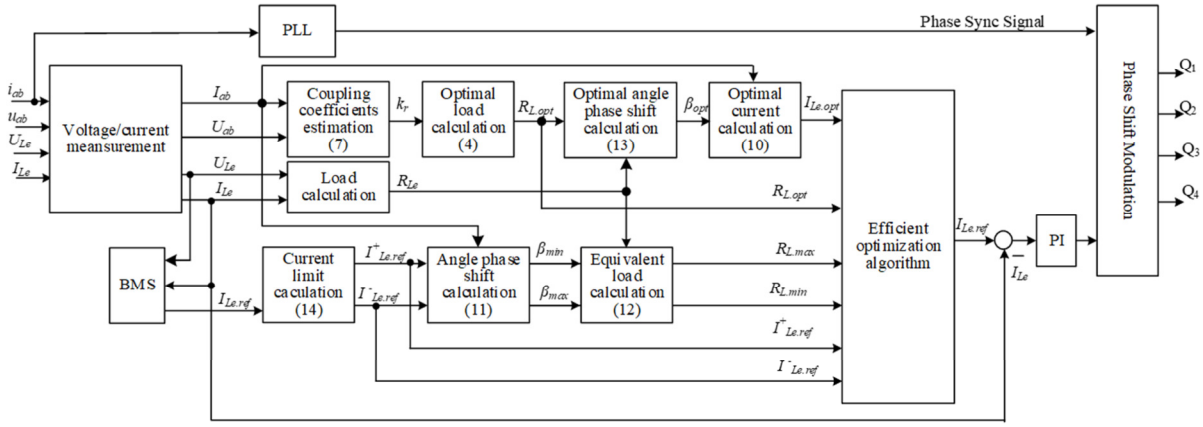

Fig. 6. The block diagram of the CC charging control combined with optimal impedance tracking.

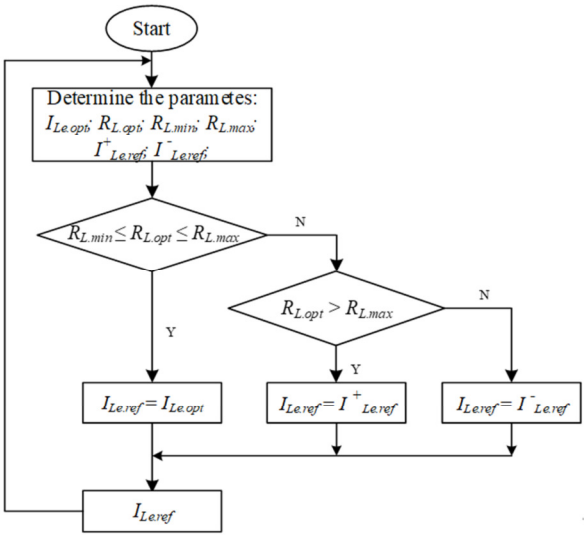

Fig. 7. Flow chart for the efficiency optimization algorithm.

IV. SIMULATION AND EXPERIMENTAL RESULTS

To verify the accuracy of the proposed method, a simulation model was built on PSIM according to Table I.

TABLE I. SYSTEM PARAMETERS

Parameter	Value	Parameter	Value
P_0	1.5 kW	L_{fi}	52.6 µH
U_{DC}	310 V	C_{fi}	66.5 nF
U_{Le}	400 V	C_1	93.7 nF
f_{sw}	85 kHz	C_2	123.2 nF
L_i	102 µH	C_3	95 nF
R_i	0.13 Ω	L_{fr}	28.9 µH
L_r	120 µH	C_{fr}	120.9 nF
R_r	0.13 Ω	C_r	38.5 nF

When the reference charging current ($I_{Le.ref}$) is 4.5A, the tolerable charging fluctuation rate δ is 5%. Figure 8 shows the simulation results when the equivalent load changes. The equivalent load (R_{Le}) increases from 70 Ω to 90 Ω and 100Ω, the charging current follows the referent within the allowable range (4.75 A, 4.5 A, and 4.25 A), the charging voltage increases respectively (332.5 V, 405 V, and 425 V), and the

average system efficiency is more than 81%. Thus, the simulation results of the CC charging process are consistent with the efficiency optimization algorithm presented in Section III(B). Figure 9 shows the dynamic charging model built in the laboratory with 1.5kW, 150mm transfer distance, and 85kHz working frequency built in the laboratory. The coils were built-in stranded wire. Polypropylene film capacitors were used to reduce losses and increase bearing capacity at high currents and frequencies. PE40 ferrite bars were used to increase magnetic conductivity. CMF20120D SIC MOSFETs were used to increase the converter efficiency.

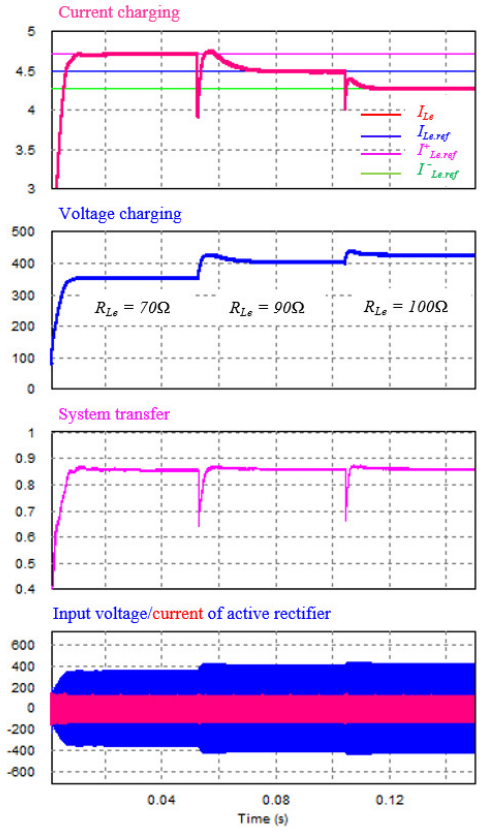

Fig. 8. Current/voltage waveforms and system efficiency when equivalent load changes.

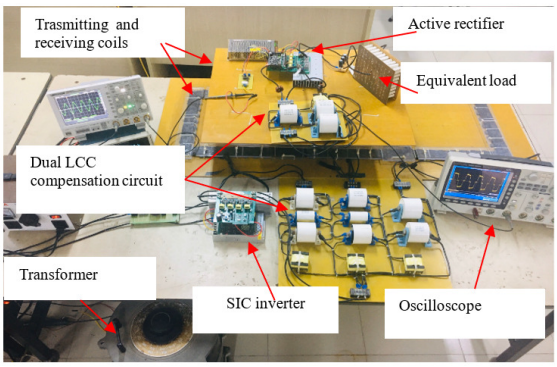

Fig. 9. The experimental model.

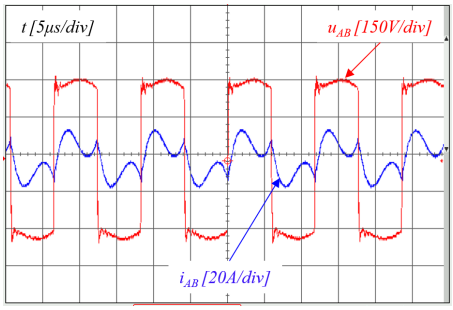

Fig. 10. Output voltage/current of 85 kHz inverter.

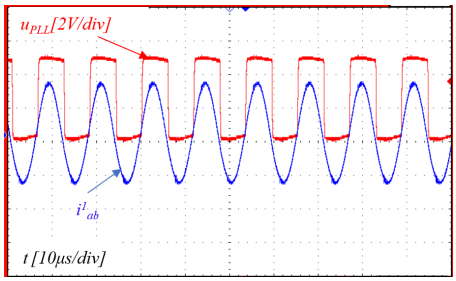

Fig. 11. Input/output signal of PLL circuit.

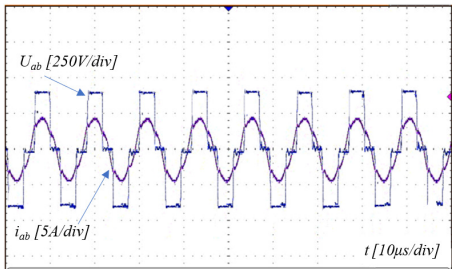

Fig. 12. Active rectifier voltage/current waveform.

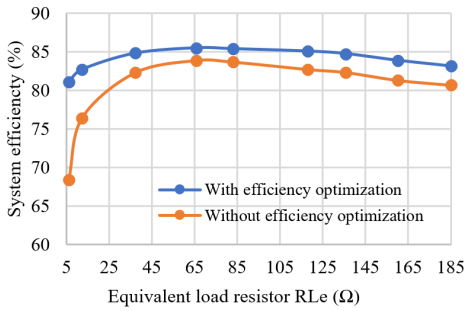

Fig. 13. System efficiency characteristics when CC charging.

Figure 10 shows the output voltage/current of the inverter. The results show that the resonant frequency is 85 kHz and that the ZVS condition for MOSFETs was achieved. Figure 11 is the result of measuring the input/output signal of the PLL circuit. The results show that the output pulse of the PLL circuit accurately captures the phase angle of the current. The pulse goes high when the current cuts through the zero point from negative to positive and goes low when the current cuts through the zero point from positive to negative. Figure 12 shows the active rectifier voltage/current waveform. The results show that the voltage and current are phase-synchronized.

Figure 13 shows the system efficiency when the receiving coil is centered on the first transmitting coil (T1), (p_x, p_y) = (0, 0), and the equivalent load varies. In case 1, without an efficiency optimization algorithm, the system efficiency was highest at an equivalent load R_{Le} of around 65Ω. When the equivalent load increases or decreases, the system efficiency decreases. In case 2, with an efficiency optimization algorithm, the system efficiency was over 82% in a wide range of equivalent loads. Thus, when applying the efficiency optimization algorithm, the efficiency was raised above 3%. The maximum system efficiency achieved was 85%.

V. CONCLUSION AND FUTURE WORK

This study implemented CC charge control with an efficiency optimization algorithm. The BMS calculates the required current charge. Then, the tolerable charging current fluctuation rate is set up. The optimal load impedance is calculated based on the previously estimated coupling coefficient. Limit load impedance values were also calculated. An efficient optimization algorithm was implemented to calculate the reference current applied to the charging current control loop. When applying the efficiency optimization algorithm, the efficiency increased by more than 3%, and the maximum efficiency achieved was 85%. Future research will focus on CV charging control to further improve the system.

ACKNOWLEDGMENT

This research was funded by the Hanoi University of Industry under project number 19 -2021-RD/HĐ-ĐHCN.

REFERENCES

[1] K. Unni and S. Thale, "Energy Consumption Analysis for the Prediction of Battery Residual Energy in Electric Vehicles," *Engineering, Technology & Applied Science Research*, vol. 13, no. 3, pp. 11011–11019, Jun. 2023, https://doi.org/10.48084/etasr.5868.

[2] N. T. Diep and N. K. Trung, "Transmitting Side Power Control for Dynamic Wireless Charging System of Electric Vehicles," *Engineering, Technology & Applied Science Research*, vol. 12, no. 4, pp. 9042–9047, Aug. 2022, https://doi.org/10.48084/etasr.4988.

[3] M. E. Bendib and A. Mekias, "Solar Panel and Wireless Power Transmission System as a Smart Grid for Electric Vehicles," *Engineering, Technology & Applied Science Research*, vol. 10, no. 3, pp. 5683–5688, Jun. 2020, https://doi.org/10.48084/etasr.3473.

[4] J. A. Sanguesa, V. Torres-Sanz, P. Garrido, F. J. Martinez, and J. M. Marquez-Barja, "A Review on Electric Vehicles: Technologies and Challenges," *Smart Cities*, vol. 4, no. 1, pp. 372–404, Mar. 2021, https://doi.org/10.3390/smartcities4010022.

[5] G. A. Covic and J. T. Boys, "Modern Trends in Inductive Power Transfer for Transportation Applications," *IEEE Journal of Emerging and Selected Topics in Power Electronics*, vol. 1, no. 1, pp. 28–41, Mar. 2013, https://doi.org/10.1109/JESTPE.2013.2264473.

[6] C. Panchal, S. Stegen, and J. Lu, "Review of static and dynamic wireless electric vehicle charging system," *Engineering Science and Technology, an International Journal*, vol. 21, no. 5, pp. 922–937, Oct. 2018, https://doi.org/10.1016/j.jestch.2018.06.015.

[7] M. A. Hannan, M. S. H. Lipu, A. Hussain, and A. Mohamed, "A review of lithium-ion battery state of charge estimation and management system in electric vehicle applications: Challenges and recommendations," *Renewable and Sustainable Energy Reviews*, vol. 78, pp. 834–854, Oct. 2017, https://doi.org/10.1016/j.rser.2017.05.001.

[8] S. Li and C. C. Mi, "Wireless Power Transfer for Electric Vehicle Applications," *IEEE Journal of Emerging and Selected Topics in Power Electronics*, vol. 3, no. 1, pp. 4–17, Mar. 2015, https://doi.org/10.1109/JESTPE.2014.2319453.

[9] T. C. Beh, T. Imura, M. Kato, and Y. Hori, "Basic study of improving efficiency of wireless power transfer via magnetic resonance coupling based on impedance matching," in *2010 IEEE International Symposium on Industrial Electronics*, Bari, Italy, Jul. 2010, pp. 2011–2016, https://doi.org/10.1109/ISIE.2010.5637484.

[10] Y. Lim, H. Tang, S. Lim, and J. Park, "An Adaptive Impedance-Matching Network Based on a Novel Capacitor Matrix for Wireless Power Transfer," *IEEE Transactions on Power Electronics*, vol. 29, no. 8, pp. 4403–4413, Dec. 2014, https://doi.org/10.1109/TPEL.2013.2292596.

[11] Y. Huang, N. Shinohara, and T. Mitani, "Theoretical analysis on DC-DC converter for impedance matching of a rectifying circuit in wireless power transfer," in *2015 IEEE International Symposium on Radio-Frequency Integration Technology (RFIT)*, Sendai, Japan, Dec. 2015, pp. 229–231, https://doi.org/10.1109/RFIT.2015.7377943.

[12] N. T. Diep, N. K. Trung, and T. T. Minh, "Maximum Efficiency in the Dynamic Wireless Charging Systems of Electric Vehicles," in *2019 10th International Conference on Power Electronics and ECCE Asia (ICPE 2019 - ECCE Asia)*, Busan, Korea (South), Feb. 2019, pp. 1–6, https://doi.org/10.23919/ICPE2019-ECCEAsia42246.2019.8797184.

[13] M. Fu, C. Ma, and X. Zhu, "A Cascaded Boost–Buck Converter for High-Efficiency Wireless Power Transfer Systems," *IEEE Transactions on Industrial Informatics*, vol. 10, no. 3, pp. 1972–1980, Dec. 2014, https://doi.org/10.1109/TII.2013.2291682.

[14] W. X. Zhong and S. Y. R. Hui, "Maximum Energy Efficiency Tracking for Wireless Power Transfer Systems," *IEEE Transactions on Power Electronics*, vol. 30, no. 7, pp. 4025–4034, Jul. 2015, https://doi.org/10.1109/TPEL.2014.2351496.

[15] T. D. Yeo, D. Kwon, S. T. Khang, and J. W. Yu, "Design of Maximum Efficiency Tracking Control Scheme for Closed-Loop Wireless Power Charging System Employing Series Resonant Tank," *IEEE Transactions on Power Electronics*, vol. 32, no. 1, pp. 471–478, Jan. 2017, https://doi.org/10.1109/TPEL.2016.2523121.

[16] Y. Chen, H. Zhang, S.-J. Park, and D.-H. Kim, "A Switching Hybrid LCC-S Compensation Topology for Constant Current/Voltage EV Wireless Charging," *IEEE Access*, vol. 7, pp. 133924–133935, 2019, https://doi.org/10.1109/ACCESS.2019.2941652.

[17] V. B. Vu, D. H. Tran, and W. Choi, "Implementation of the Constant Current and Constant Voltage Charge of Inductive Power Transfer Systems With the Double-Sided LCC Compensation Topology for Electric Vehicle Battery Charge Applications," *IEEE Transactions on Power Electronics*, vol. 33, no. 9, pp. 7398–7410, Sep. 2018, https://doi.org/10.1109/TPEL.2017.2766605.

[18] K. Song, Z. Li, J. Jiang, and C. Zhu, "Constant Current/Voltage Charging Operation for Series–Series and Series–Parallel Compensated Wireless Power Transfer Systems Employing Primary-Side Controller," *IEEE Transactions on Power Electronics*, vol. 33, no. 9, pp. 8065–8080, Sep. 2018, https://doi.org/10.1109/TPEL.2017.2767099.

[19] Z. Li, K. Song, J. Jiang, and C. Zhu, "Constant Current Charging and Maximum Efficiency Tracking Control Scheme for Supercapacitor Wireless Charging," *IEEE Transactions on Power Electronics*, vol. 33, no. 10, pp. 9088–9100, Jul. 2018, https://doi.org/10.1109/TPEL.2018.2793312.

[20] G. Graber, V. Galdi, V. Calderaro, and A. Piccolo, "A power split control algorithm for fuel cell electric vehicles using batteries or supercapacitors as auxiliary storage system," in *2017 6th International Conference on Clean Electrical Power (ICCEP)*, Santa Margherita Ligure, Italy, Jun. 2017, pp. 625–630, https://doi.org/10.1109/ICCEP.2017.8004754.

[21] Y. Li, J. Hu, F. Chen, Z. Li, Z. He, and R. Mai, "Dual-Phase-Shift Control Scheme With Current-Stress and Efficiency Optimization for Wireless Power Transfer Systems," *IEEE Transactions on Circuits and Systems I: Regular Papers*, vol. 65, no. 9, pp. 3110–3121, Sep. 2018, https://doi.org/10.1109/TCSI.2018.2817254.

[22] N. T. Diep, N. K. Trung, and T. T. Minh, "Wireless power transfer system design for electric vehicle dynamic charging application," *International Journal of Power Electronics and Drive Systems (IJPEDS)*, vol. 11, no. 3, pp. 1468–1480, Sep. 2020, https://doi.org/10.11591/ijpeds.v11.i3.pp1468-1480.